Contrasting Behaviors between the Rapidly Intensifying and Slowly Intensifying Tropical Cyclones in the North Atlantic and Eastern Pacific Basins

XINXI WANG[a] AND HAIYAN JIANG[a]

[a] *Department of Earth and Environment, Florida International University, Miami, Florida*

(Manuscript received 7 December 2019, in final form 29 October 2020)

ABSTRACT: Based on 35-yr (1982–2016) best track and Statistical Hurricane Intensity Prediction Scheme data, this study examined climatology of rapidly intensifying (RI) and slowly intensifying (SI) events as well as their time evolutions of storm-related and environmental parameters for tropical cyclones (TCs) in both North Atlantic (AL) and eastern North Pacific (EP) basins. Major hurricanes were intensified mainly through RI while tropical depression and tropical storms were intensified through SI. The percentage of TCs that underwent RI peaks in the late hurricane season whereas the percentage of TCs that underwent SI peaks early. For the first time in the literature, this study found that RI events have significantly different storm-related and environmental characteristics than SI events for before-, during-, and after-event stages. In both AL and EP basins, RI events always intensify significantly faster during the previous 12 h, are located farther south, and have warmer sea surface and 200-hPa temperatures, greater ocean heat content, larger 200-hPa divergence, weaker vertical wind shear, and weaker 200-hPa westerly flow than SI events for all event-relative stages. In the AL basin, RI events have larger low-level and midlevel relative humidity and larger 850-hPa relative vorticity than SI events for all event-relative stages in the AL and most event-relative stages in the EP. RI events are associated with more convectively unstable atmosphere and are farther away from their maximum potential intensities than SI events for most event-relative stages in the AL and for all event-relative stages in the EP.

KEYWORDS: Tropical Cyclones; Climatology; Storm Environment; Statistics

1. Introduction

While the operational track prediction of tropical cyclones (TCs) have improved substantially during the past a few decades, the prediction of TC intensity change, especially rapid intensification (RI), remains one of the greatest challenges for both the forecasting and research communities (DeMaria et al. 2014). It is widely accepted that the necessary condition for TC intensification is a favorable preexisting environmental condition including warm sea surface temperature (SST), low vertical wind shear, and high lower-tropospheric relative humidity (Merrill 1988; Kaplan and DeMaria 2003, hereafter KD03; Kaplan et al. 2010). One of the major unanswered scientific questions is how to better forecast RI, especially when the environmental conditions are favorable for TC intensification in general, including RI and slow intensification (SI). Previous studies have demonstrated that some of the storm-related and large-scale environmental parameters, such as sea surface temperature, vertical wind shear, 200-hPa zonal wind, and low-level relative humidity, in RI cases are significantly different with those in non-RI cases in both the North Atlantic (AL, KD03) and the western North Pacific (WP; Shu et al. 2012) basins. The Statistical Hurricane Intensity Prediction Scheme (SHIPS; DeMaria and Kaplan 1994, 1999; DeMaria et al. 2005; DeMaria 2010; Schumacher et al. 2013) RI index was developed based on a set of storm-related and environmental predictors for AL and eastern North Pacific (EP) basins, respectively (Kaplan et al. 2010, 2015).

Although it is relatively easy to distinguish RI from non-RI cases using storm-related and environmental parameters, the problem becomes more difficult when distinguishing RI from SI cases. Hendricks et al. (2010, hereafter HPFL10) showed that environmental characteristics are similar when comparing RI with SI cases in the AL and WP basins. The only exceptions were that in the AL basin, the environmental vertical wind shear was found to be significantly weaker in RI than SI cases; while in the WP basin, the conditional instability was significantly larger for RI than SI cases.

KD03 first defined RI as a future 24-h period with intensity increase greater than 30 kt (1 kt = 0.5144 m s^{-1}), which is equivalent to the 95th percentile of the future 24-h intensity change. This RI threshold has been adopted by many following studies. KD03 treated each 24-h RI period as an independent case. All above-mentioned environmental-based RI studies (KD03; Kaplan et al. 2010; HPFL10; Shu et al. 2012) adopted this RI case-based definition, as well as some satellite-based statistical RI studies (DeMaria et al. 2012; Jiang and Ramirez 2013; Zagrodnik and Jiang 2014; Alvey et al. 2015; Tao and Jiang 2015). Each 24-h period has been treated as an independent RI case from others in the studies above. However, in reality, RI occurs as an even, which could last for more than 48–60 h (Kieper and Jiang 2012). Treating each 24-h RI period as an independent case could be problematic because it does not take the storm evolution information into account.

Tao et al. (2017, hereafter TJZ17) first proposed the RI event-based definition. In their definition, each RI event contains multiple, continuous, and overlapping 24-h RI cases. For each RI event, different stages were further classified, including "Before RI," "During RI," "RI ending," and "After RI."

Corresponding author: Haiyan Jiang, haiyan.jiang@fiu.edu

DOI: 10.1175/JCLI-D-19-0908.1

This event-based RI definition favors the analysis of evolution of environmental or storm properties with respect to RI events. Using this RI event definition and the Tropical Rainfall Measuring Mission (TRMM) Tropical Cyclone Precipitation Feature (TCPF) database (Jiang et al. 2011), TJZ17 found that a progressive increase in the occurrence and azimuthal coverage of stratiform rainfall during the RI events, especially in the upshear-left quadrant.

RI is found not to be caused by special processes in the atmosphere but is part of a continuum of TC intensification (Kowch and Emanuel 2015). This intensification has been linked with environmental factors and TC internal processes. Recently, advances on the external and environmental influences on tropical cyclone intensification rate change has been achieved. These external influences include SST, ocean heat content (OHC), vertical wind shear, relative humidity of the environmental air, trough interaction measured by divergence and vorticity, and other multiple factors that may impact TC intensity change. Each environmental factor and TC intensification rate relationships vary from basin to basin. The contribution of SST is found to be much higher in the EP basin than in the AL basin (Foltz et al. 2018). While the variability of SST is lower in the AL alone TC track than in the Pacific, the gradients in OHC are larger. While large OHC gradients directly cause strong air–sea interaction, which provide more energy to TC, SST tends to be vary associated with vertical wind shear pattern and TC outflow temperature. Vertical wind shear is one of the most dominant factors on TC intensity. It cannot only influence on convection and precipitation within TC (Tao and Jiang 2015), which can make feedback to TC intensity (Nguyen and Molinari 2015), but also directly effect on TC vortices and intensity (Gu et al. 2016; Zhang et al. 2015). The location of environmental dry air inflow and how it interacts with TC circulation are related to TC intensification. Environmental dry air might not influence TC intensification processes if it cannot get entangled into TC inner core (Bukunt and Barnes 2015), while it is related with TC intensification if it located ahead of TCs (Wu et al. 2015; Ditchek et al. 2017). Other weather systems like trough and upper-level jet could also be factor on TC intensification. The eddy flux convergence, which is an additional mechanism by which environmental angular momentum associated with a trough, could be a factor to positively or negatively influence TC intensity (DeMaria et al. 1993; Hanley et al. 2001; Peirano et al. 2016). However, the physical relationships between RI and those environmental factors are remain problematics. For example, the starting time of RI is always uncertainty due to complex interaction between vertical wind shear, TC vortex, and convection (Judt and Chen 2016). Increased understanding on explaining the physical relationship between environmental controls and TC intensification process is needed. In this study, observation environmental parameters are used to show the relationship between environmental controls and RI or SI events.

In this study, an event-based definition similar as in TJZ17 is applied to both RI and SI events in TCs in AL and EP basins during a 35-yr period (1982–2016). One objective of this study is to compare the evolution of environmental parameters during RI and SI events. We would like to verify if HPFL10 results are still valid when treating RI and SI as events. Both RI and SI events will be classified into before, during and after RI/SI stages. We seek to answer this important question, "*Are there any differences of various environmental parameters between corresponding stages for RI versus SI events?*" The environmental parameters in TCs will be derived from the SHIPS developmental dataset.

Another objective of this study is to examine the 35-yr climatology of RI/SI storms and events in AL and EP basins. The climatology of RI has been documented in different TC-prone basins and for various time periods. Table 1 is a summary of recent studies on RI climatology (KD03; Kaplan et al. 2010; HPFL10; Shu et al. 2012; Wang et al. 2015, Fudeyasu et al. 2018; Zhao et al. 2018; Leroux et al. 2018). All these studies used the 24-h RI case-based definition as in KD03. In these studies, RI storms were defined as TCs that underwent at least one 24-h RI period during their life cycle. It was found that as the maximum lifetime intensity (LMI) of TCs increases, the percentage of TCs undergoing RI increases as well. For example, KD03 showed that 31% of all TCs, 60% of all hurricanes, 83% of all major hurricanes, and 100% of category 4 and 5 hurricanes underwent RI at least once during their lifetimes for TCs in the AL basin during 1989–2000. Similar results were found for TCs in WP (Shu et al. 2012) and the southwest Indian Ocean (SWIO, Leroux et al. 2018) basins. RI cases are usually concentrated between 10° and 20°S or between 10° and 20°N (HPFL10; Shu et al. 2012; Wang et al. 2015, Fudeyasu et al. 2018; Zhao et al. 2018; Leroux et al. 2018), except that in the AL basin RI cases could occur anywhere between 10° and 30°N (KD03; Kaplan et al. 2010; HPFL10; Wang et al. 2017). In the Northern Hemisphere, RI usually peaks in August and September (KD03; Kaplan et al. 2010; Shu et al. 2012; Wang et al. 2015; Fudeyasu et al. 2018; Zhao et al. 2018), while in the Southern Hemisphere RI storms distribute almost evenly between October and May (Leroux et al. 2018). In this study, instead of using the RI case-based definition as all these previous RI climatology studies, we will use the RI/SI event-based definition to examine and compare the climatology of RI/SI storms and events in AL and EP basins.

This paper is organized as follow. Section 2 describes the data and methodology used in this study. The climatology of RI and SI events and storms is presented in section 3. A comparison of large-scale environmental conditions associated with RI and those associated with SI events is presented in section 4.

2. Data and methodology

a. Identifying RI and SI events from the best track data

The dataset for this study contains TCs in AL and EP basins during 1982–2016. The best track database HURDAT2 (Landsea and Franklin 2013) from the National Hurricane Center (NHC) is used for TC center position and intensity. The HURDAT2 data include nondeveloping depressions. In this study, all nondeveloping depressions and named TCs are included, similar as KD03. The maximum sustained surface wind

TABLE 1. The geographical region of RI occurrence and seasonal distribution of RI storms by previous studies with respect to their analysis periods and their study basins.

Basin	Studies	Analysis period	RI threshold (95th percentile	RI zone (percentage of RI storms)	Seasonal distribution (percentage of RI storms)
AL	Kaplan and DeMaria (2003)	1989–2000 (12 years)	30 kt	10°–30°N, 20°–97°W	Jun–Jul (5%), Aug–Sep (72%), Oct–Nov (23%)
	Kaplan et al. (2010)	1989–2006 (18 years)	30 kt	10°–30°N, 20°–97°W	Jun–Jul (11%), Aug–Sep (67.7%), Oct–Nov (22%)
	Hendricks et al. (2010)	2003–08 (6 years)	35 kt	10°–30°N, 20°–97°W	—
EP	Kaplan et al. (2010)	1989–2006 (18 years)	35 kt	10°–20°N, 95°–140°W (94% of RI)	Jun–Jul (32%), Aug–Sep (51%), Oct–Nov (16%)
WP	Hendricks et al. (2010)	2003–08 (6 years)	38 kt	10°–25°N, 125°–140°E	—
	Shu et al. (2012)	1970–2007 (28 years)	20 kt	10°–20°N, 127°–143°E	Jul (17%), Aug (16%), Sep (20%), Oct (18%)
	Wang et al. (2015)	1951–2008 (48 years)	30 kt	8°–20°N, 125°–155°E (68% of RI)	May–Nov (92%, peak in Aug)
	Fudeyasu et al. (2018)	1979–2015 (37 years)	30 kt	9°–21°N, 121°–143°E	Peak in Sep
	Zhao et al. (2018)	1979–2015 (37 years)	30 kt	10°–22°N, 120°–155°E (60% of RI)	Jul–Nov (81%, peak in Sep)
SWIO	Leroux et al. (2018)	1999–2016 (18 years)	30 kt	10°–20°S, 50°–95°E	Oct–May

speed is treated as the intensity metric. Only records of tropical depression intensity or stronger are retained. The 6-h best track records (containing synoptic time of 0000, 0600, 1200, and 1800 UTC) in which the TC had land interaction within 24 h and cases where the TC was positioned north of 30°N have been removed. The remaining best track records, containing a total of 997 TCs, including 439 in AL and 558 in EP (Table 2), are used to calculate the 24-h future TC intensity change (ΔV_{24}).

The filtered dataset yields 13 730 and 16 283 intensity change estimates for AL and EP, respectively. Next, we will use these ΔV_{24} estimates to define RI and SI events by following TJZ17. Each RI or SI event contains one or more continuous and overlapping 24-h periods during which the 24-h intensity change ΔV_{24} meets the RI or SI criterion, respectively. The RI threshold is chosen as the 95th percentile of ΔV_{24} for all the TC best track records selected in this study by following KD03. Figure 1 demonstrated that the 95th percentile of the 24-h future intensity change is 30 kt for the TC dataset used in this study. This is consistent with many previous studies that found that the same 30 kt threshold can be used globally (Jiang 2012; Jiang and Ramirez 2013; Zagrodnik and Jiang 2014) or for

TABLE 2. Numbers and percentages (in parentheses) of RI and SI storms in different TC LMI categories over the North Atlantic (AL) and eastern North Pacific (EP) basins during 1982–2016.

		AL	EP	TOTAL
TD/TS	Total count	214	240	454
	RI (%)	6 (2)	4 (1)	10 (2)
	SI (%)	124 (58)	199 (83)	323 (72)
CAT12	Total count	133	159	292
	RI (%)	47 (35)	82 (52)	129 (44)
	SI (%)	62 (47)	77 (48)	140 (48)
CAT35	Total count	92	159	251
	RI (%)	79 (86)	147 (92)	226 (90)
	SI (%)	12 (13)	12 (8)	24 (10)
ALL	Total count	439	558	997
	RI (%)	132 (30)	233 (42)	365 (37)
	SI (%)	198 (45)	288 (52)	486 (49)

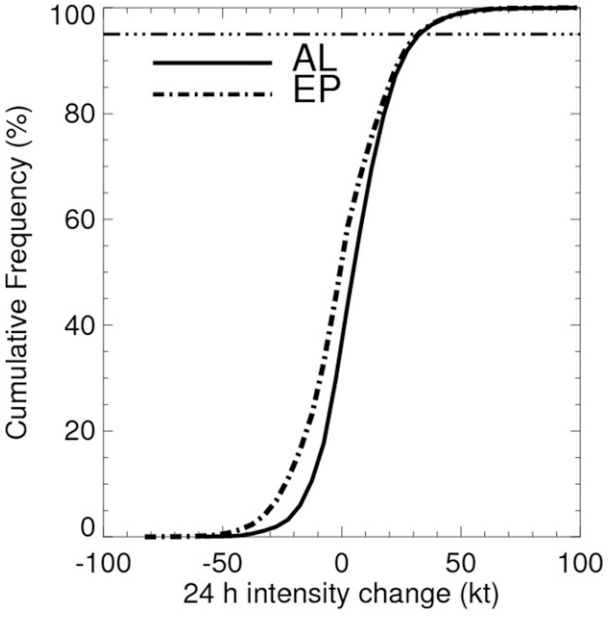

FIG. 1. Cumulative density function (CDF) of the overwater 24-h intensity changes of the 1982–2016 AL and EP samples.

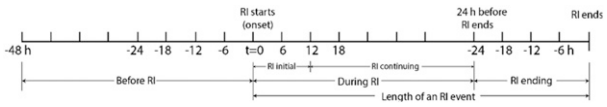

FIG. 2. Schematic of before-RI, RI-initial, RI-continuing, and RI-ending periods within a typical RI event defined using the best track data (adapted from Tao et al. 2017).

individual basins such as AL (KD03; Kaplan et al. 2010), WP (Shu et al. 2012; Wang et al. 2015; Fudeyasu et al. 2018; Zhao et al. 2018), and SWIO (Leroux et al. 2018). However, there are some exceptions. HPFL10 found that the 95th percentile of ΔV_{24} was 35 kt for AL TCs and 38 kt for EP TCs during a 5-yr period (2003–08). Similarly, Kaplan et al. (2010) found that the 95th percentile of ΔV_{24} was 35 kt for AL TCs during an 18-yr period (1989–2006). HPFL10 study period is much shorter than other studies mentioned above, which might be the main reason for their higher RI threshold. This study uses a longer period (35 years) than Kaplan et al. (2010) study, which again might be the reason that the RI threshold for EP decreases from 35 kt in Kaplan et al. (2010) to 30 kt in this study.

Therefore, an RI threshold of $\Delta V_{24} \geq 30$ kt is employed in this study to identify RI events. To identify SI events, the SI threshold is chosen to be $10 \leq \Delta V_{24} < 30$ kt, by following Jiang and Ramirez (2013). To clarify, any TCs with $\Delta V_{24} \geq 10$ kt will be identified as either RI or SI storms.

An automatic method was developed by TJZ17 and adapted in this study to identify RI and SI events from the best track data. As illustrated in Fig. 2, the onset of an RI event (''RI starts'' on Fig. 2) is the starting time of the first 24-h RI period within the RI event. The ending time of an RI event (''RI ends'' on Fig. 2) is the ending time of the last 24-h RI period within the RI event. The length of an RI event is the total time length between RI onset and RI ending time points. Each 24-h RI period within an RI event corresponds to one RI case as in KD03 and other RI case-based studies. The onset and ending time and the length of SI events are defined similar as RI events by using the SI threshold $10 \leq \Delta V_{24} < 30$ kt. The minimum length of RI/SI event is 24 h. As shown in Table 3, the maximum length of an RI event is 78 h, while the maximum length of an SI event is 144 h. Each RI (SI) storm could have multiple RI (SI) events. In this study, 428 RI events and 670 SI events are statistically identified based on best track 6-hourly dataset out of 365 RI storms and 486 SI storms, respectively (Table 3).

To study the evolution of RI and SI events, we classify different stages associated with each RI or SI event. Similar with TZJ17, these stages include ''before RI/SI,'' ''during RI/SI (between RI/SI onset and 24 h before RI/SI ends),'' and ''RI/SI ending (the last 24 h of the RI/SI event).'' Note that all the ''during RI/SI'' samples must be at least 24 h before RI/SI ends. This ensures that each during-RI/SI sample is an RI/SI case that meets the 24-h future intensity change criterion. Instead, the RI/SI ending stage contains a 24-h period during which the 24-h future intensity change ΔV_{24} does not meet the RI/SI threshold anymore. The best track sample sizes for different time periods associated with RI/SI events identified in this study are shown in Table 4.

b. *Examining storm-related and environmental parameters from SHIPS database*

Table 5 lists the storm-related, and environmental parameters for each 6-h data point for all TCs to be analyzed in this study. These parameters are derived from the HURDAT2 file (https://www.nhc.noaa.gov/data/) and SHIPS developmental database (http://rammb.cira.colostate.edu/research/tropical_cyclones/ships/developmental_data.asp). The SHIPS data contain synoptic information every 6 h (0000, 0600, 1200, and 1800 UTC) for AL TCs and EP TCs from 1982 to 2016. In this study, we only used the 0000 UTC synoptic information (from model initialization by observations) for each best track data point.

The storm-related parameters of TCs (first 6 parameters of Table 5) are determined directly from the HURDAT2 file, including the storm's maximum sustained surface wind speed (VMX), center position including latitude (LAT) and longitude (LON), storm speed of motion (SPD), u component of storm motion (USTM), and intensity change during the previous 12 h (DVMX). SPD and USTM are computed for the 12-h period centered on the initial ($t = 0$ h) time of each 24-h period, same as in KD03. DVMX is evaluated by subtracting VMX at $t = 0$ h from VMX at $t = -12$ h.

The rest of parameters in Table 5 are environmental parameters from SHIPS. All the SHIPS parameters were from National Center for Atmospheric Research (NCEP) global model analyses (either reanalysis or operational). Since SHIPS is a statistical prediction model, the SHIPS database contains a time series of each parameter from the initial time ($t = 0$ h) to $t = 120$ h in the future. In this study, we only use each parameter's value at initial time ($t = 0$ h). A detailed description on how each SHIPS parameter is calculated can be found in previous SHIPS documents. Briefly, the sea surface temperature (SST) was derived from the Reynolds and Smith (1993) gridded 1.0°latitude-longitude weekly analysis available prior to storm passage. The magnitudes of 850–700-hPa relative humidity (RHLO), the 700–500-hPa relative humidity (RHMD),

TABLE 3. Number and percentage (in parentheses) of RI/SI events in each event length category in AL and EP basins during 1982–2016.

		Event length (h)										
		24	30	36	42	48	54	60	66	72	78–144	ALL
AL	RI (%)	41 (25)	39 (24)	29(18)	27 (17)	14 (9)	8 (5)	1 (1)	0 (0)	0 (0)	1 (1)	160
	SI (%)	68 (24)	53 (19)	42 (15)	45 (16)	25 (9)	15 (5)	9 (3)	12 (4)	4 (1)	11 (4)	284
EP	RI (%)	55 (21)	51 (19)	36 (14)	52 (19)	25 (9)	22 (8)	14 (5)	8 (3)	4 (2)	1 (0)	268
	SI (%)	80 (21)	59 (15)	58 (15)	57 (15)	33 (9)	22 (6)	20 (5)	13 (3)	12 (3)	32 (8)	386

TABLE 4. Number of selected best track data points in different time periods before RI/SI, during RI/SI, and in the RI/SI ending stage for RI/SI events in AL and EP basins during 1982–2016.

		Before-event (hours before onset)						During-event (hours after onset)				Event-ending (hours before event ends)				
								Initial		Continuing						
Stages		36–48 h	24–36 h	18–24 h	12–18 h	6–12 h	0–6 h	0–6 h	6–12 h	12–18 h	18–84 h	18–24 h	12–18 h	6–12 h	0–6 h	ALL
RI	AL	94	118	77	90	110	124	160	119	80	90	139	119	98	44	1462
	EP	131	185	124	152	182	228	268	213	162	295	263	250	242	99	2794
SI	AL	62	92	61	80	103	143	284	216	163	353	218	169	153	83	2180
	EP	80	126	94	113	141	170	386	306	247	693	379	346	330	121	3532
RI	AL			613						449			400			1462
	EP			1002						938			854			2794
SI	AL			541						1016			623			2180
	EP			724						1632			1176			3532

u component of the 200-hPa wind (U200), and the 200-hPa temperature (T200) were computed by averaging each of these variables from radius (r) = 200–800 km. The magnitudes of 200-hPa divergence (D200) and 850-hPa vorticity (Z850) were obtained by averaging each of these variables from r = 0–1000 km. The environmental vertical wind shear (SHRD) was determined by subtracting the 850- and 200-hPa wind vectors averaged from r = 200–800 km. The storm potential parameter (POT) was determined by subtracting VMX at t = 0 h from the empirical maximum potential intensity (MPI). The methodology used to compute the relative eddy flux convergence (REFC) is the same as described in KD03. In recent years, more parameters have been added to the SHIPS database. Among them, the following parameters are analyzed in this study: the oceanic heat content (OHC), total precipitable water (MTPW, averaged within 0–500 km from the storm center), and average potential temperature θ_e difference between a parcel lifted from the surface and its environment (EPOS, averaged for r = 200–800 km).

3. Climatology of RI/SI storms and events in the AL and EP basins

In this study, RI storms are defined as TCs undergoing at least one 24-h RI period during their lifetimes. SI storms must be *non-RI storms* undergoing at least one 24-h SI period during their lifetimes. Table 2 lists the numbers and percentages of RI and SI storms for all TCs and TCs with LMI at tropical depression and tropical storm (TD/TS), category-1–2 (CAT12) hurricane, and category-3–5 (CAT35) hurricane categories on the Saffir–Simpson hurricane scale (Simpson 1974), respectively. During the 35-yr (1982–2016) study period, there are 132 RI and 198 SI storms out of a total of 439 TCs identified in the AL basin during the 35-yr study period. In the EP basin, there are 233 RI and 288 SI storms out of a total of 558 TCs (Table 2). In general, EP TCs have a larger fraction that underwent either RI or SI than AL TCs. In the AL basin, 30% of TCs underwent RI and 45% SI. But in the EP, 42% of TCs underwent RI and 52% SI. As mentioned in Kaplan et al. (2010), this might be due to "a higher probability of capturing the entire life cycle of EP systems due to the lower likelihood of systems making landfall or becoming extratropical in that basin." For both basins, 37% of all TCs underwent RI and 49% SI. Breaking down to each LMI category, 2% of all TD/TS systems, 44% of all CAT12 hurricanes, and 90% of all major hurricanes underwent RI, while 72% of all TD/TS systems, 48% of all CAT12 hurricanes, and 10% of all major hurricanes underwent SI. In comparison, KD03 found that 31% of all TCs and 83% of all major hurricanes underwent RI for AL TCs during 1989–2000, while Shu et al. (2012) found that 18% of all TCs and 70% of all super typhoons underwent RI for WP TCs during 1970–2007.

Although only 1%–2% of all TD/TS systems underwent RI in both basins, TD/TS systems in EP have a much higher percentage that underwent SI than those in AL (83% vs 58%). This suggests that a large proportion (40%) of TD/TS systems in the AL basin underwent neither RI nor SI during their whole life cycle. The percentage of AL CAT12 hurricanes that underwent RI is 35% and that underwent SI is 47%. In contrast, 52% of CAT12 hurricanes in EP underwent RI, while 48% of them underwent SI. For major (CAT35) hurricanes, 92% of them underwent RI and the rest of them underwent SI in the EP basin, while in the AL basin, 86% of them underwent RI and 13% of them underwent SI. Table 2's result suggests that major hurricanes were intensified mainly through undergoing RI while TD/TS systems were intensified mainly through SI. About a half of CAT12 hurricanes intensified through RI and another half through SI.

Table 3 lists the number and percentage of RI and SI events in each event length category. The minimum length of an RI/SI event is 24 h. Such RI/SI events only contain one 24 h RI/SI period, which is equivalent to the RI/SI case-based definition as discussed in the introduction. Table 3 shows that that only 25% of RI events in the AL basin and 21% of RI events in the EP basin last only 24 h. The majority of the RI/SI events last more than 24 h. The maximum length of an RI event is 78 h, while the maximum length of an SI event is 144 h. This strongly suggests the necessity of treating RI and SI as events when examining the evolution of RI/SI. In contrast, the RI/SI case-based definition (treating each 24-h RI/SI period as an independent case) is unable to correctly classify before RI/SI, during RI/SI, and RI/SI ending stages.

Figure 3 shows the tracks of all TCs, RI events, and SI events in the AL and EP basins during 1982–2016. TCs in both basins

TABLE 5. Definitions of storm-related and synoptic variables according to SHIPS.

Variable	Unit	Definition
VMX	kt	Maximum sustained surface wind speed
LAT	°N	Latitude
LON	°E	Longitude
SPD	$m\,s^{-1}$	Storm speed of motion
DVMX	kt	Intensity change during the previous 12 h
USTM	$m\,s^{-1}$	u component of storm motion
SST	°C	Sea surface temperature
RHLO	%	850–700-hPa relative humidity (averaged for r = 200–800 km)
RHMD	%	Same as above, but for 700–500 hPa
U200	kt	200-hPa zonal wind (averaged for r = 200–800 km)
T200	°C	200-hPa temperature (averaged for r = 200–800 km)
D200	$10^{-6}\,s^{-1}$	200-hPa divergence (averaged for r = 0–1000 km)
Z850	$10^{-6}\,s^{-1}$	Same as above for 850-hPa vorticity
EPOS	°C	Average θ_e difference between a parcel lifted from the surface and its environment (averaged for r =200–800 km)
REFC	$m\,s^{-1}\,day^{-11}$	Relative eddy momentum flux convergence (averaged for r = 100–600 km)
SHRD	kt	850–200-hPa shear magnitude (averaged for r = 200–800 km)
POT	kt	Maximum potential intensity (MPI) – VMX
OHC	$K\,J\,cm^{-2}$	Ocean heat content from satellite altimetry data

mostly moved northwestward, in accordance with the prevailing environmental steering of the easterly trade winds and with the beta effect (Holland 1983; Chan and Williams 1987), before they recurved northward or northeastward for their extratropical transition, especially in the AL basin (Fig. 3a). Interestingly, both RI and SI events were mainly concentrated between 10°–20°N in the EP basin and 10°–30°N in the AL basin, although there are a little more SI events than RI events that extended to north of 20°N in EP and north of 30°N in AL (Figs. 3b,c). The RI concentration belts are similar to what were found by previous studies (KD03; Kaplan et al. 2010; HPFL10, Shu et al. 2012; Wang et al. 2015; Wang et al. 2017; Fudeyasu et al. 2018; Zhao et al. 2018; Leroux et al. 2018). During the whole life times of RI/SI events, RI events contain more time periods with storm intensity equal to or stronger than hurricane intensity (Fig. 3b), while SI events contain more time periods with storm intensity at TD/TS level (Fig. 3c).

Figure 4 presents the seasonal distribution of the number of all TCs, RI storms, and SI storms in AL and EP basins. In the AL basin, the total number of TCs peaks in September, followed by August and October. So does the number of RI storms and that of SI storms. In the EP basin, both numbers of all TCs and SI storms peak in July, followed by August and September. But the number of RI storms peaks in September instead, followed by July and August. The monthly distribution of RI and SI events is very similar to that of RI and SI storms (not shown). Previous studies found a seasonal peak of RI cases in August and September for AL TCs during a 12-yr (1989–2000) period (KD03) and an 18-yr (1989–2006) period (Kaplan et al. 2010). For the EP basin during 1989–2006, Kaplan et al. (2010) found that RI cases showed a seasonal peak in September. These are in line with the results here.

However, when examining the RI/SI storm occurrence rate relative to the total number of TCs, the seasonal peaks change dramatically in both basins. The percentage of TCs that underwent RI peaks late in the hurricane season, November in AL and December in EP (Figs. 5a,c). In contrast, the percentage of SI storms peaks early in the season, June in AL and May in EP (Figs. 5b,d). This is an interesting result that has not been documented before. The exact reason is unknown and worthy of future studies.

The characteristics of the onset and peak intensity of RI and SI events and their relationship to TC intensity change are examined in Fig. 6. The modes of the probability density functions (PDFs) of the onset VMX of RI and SI events in both AL and EP basins are around 25–30 kt, indicating that most of TCs started to either slowly or rapidly intensify in their early stage of life time (Fig. 6a). However, there is a second mode for RI events, which is about 50 kt. This indicates that an RI event can start much later in their lifetime. At such a strong intensity (around 50 kt or above), a TC has more organized convection and precipitation structures, which provides a more favorable internal dynamic condition for RI (HPFL10; Tao and Jiang 2015; TJZ17). This is why forecasters often see RI starts from even category-1–2 hurricane stages (VMX between 65 and 100 kt) as long as the environment is favorable and the storm has still not reached its maximum potential intensity (Kieper and Jiang 2012). When comparing AL and EP basins, RI and/or SI storms in AL basin generally started RI or SI in a higher onset VMX than those in EP basin (Fig. 6b). The mode of peak VMX in SI events is only 30 kt in EP, but 50 kt in AL (Fig. 6c). The maximum peak VMX for SI events in AL is much higher than that in EP as well. A TC can reach an intensity as high as 80 kt in EP, but 115 kt in AL, through a SI event. For RI events, the mode of event peak VMX has a wide range between ~65–90 kt, with the maximum event peak VMX as high as 160 kt for AL and 185 kt for EP RI events. The cumulative density functions (CDFs) of RI event peak VMX in AL and EP basins

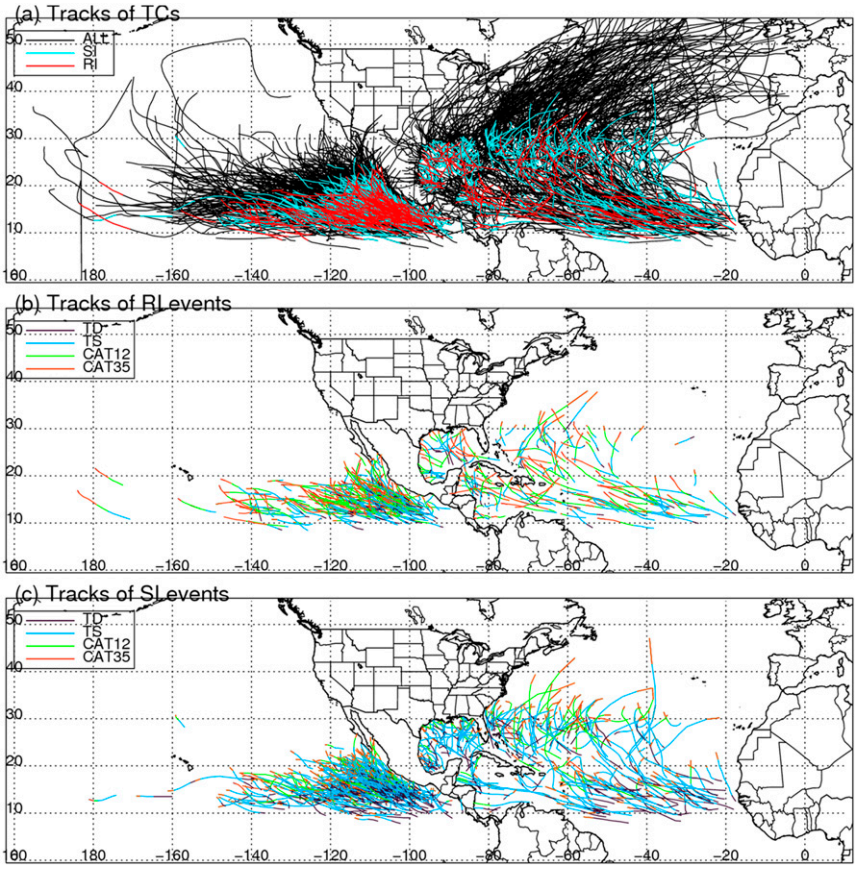

FIG. 3. (a) Tracks of TCs in the North Atlantic and eastern North Pacific basins during 1982–2016. Tracks of RI events and SI events are colored as red and cyan, respectively. (b) Tracks of RI events in the North Atlantic and eastern North Pacific basins during 1982–2016. Intensity stages of tropical depression (TD), tropical storm (TS), category-1–2 hurricane (CAT12), and category-3–5 hurricane (CAT35) are indicated in different colors. (c) As in (b), but for SI events.

are similar, while the peak intensity is much higher for SI events in AL than for those in EP (Fig. 6d).

The TC intensity increase during an RI or SI event can be indicated by the difference between peak VMX and onset VMX. As shown in the figures of PDFs and CDFs, the TC intensity increase during SI events are all less than 90 kt in the AL and the EP basins (Figs. 6e,f). On the other hand, the TC intensity increase during RI events could reach 110 kt in the AL and 150 kt in the EP basins.

4. Time evolutions of storm-related and large-scale parameters for RI and SI events and their statistical significance differences between RI and SI events

In this section, the time evolutions of storm-related and large-scale parameters (Table 2) for RI events are compared with those for SI events of non-RI storms for the AL and EP basins. The before RI/SI stage (*before-event*) is further separated into 0–6, 6–12, 12–18, 18–24, 24–36, and 36–48 h before RI/SI. The during RI/SI stage (*during-event*) is separated into RI/SI *initial* (0–6 and 6–12 h after RI/SI onset) and RI/SI *continuing* (between 12–18 h after RI/SI onset and between 18 h after RI/SI onset and 24 h before RI/SI ends). The RI/SI ending stage (*event-ending*) is further separated into 18–24, 12–18, 6–12, and 0–6 h before RI/SI ends. The sample size of each of the 14 substages is indicated in Table 4.

In Fig. 6a, two peaks of event onset VMX (VMX_{start}) are seen. We hypothesize that physical processes associated working on events with weak winds and those working on events in which RI/SI starts from strong intensity are different. Based on Fig. 6a, two groups of RI/SI events are separated using the threshold of 40 kt for VMX_{start}. One group includes events with $VMX_{start} \leq 40$ kt and the other with $VMX_{start} > 40$ kt. All the storm-related and environmental parameters are examined for each event group in all the three event-relative stages for both basins. We found that compared to the parameters for SI event, favorable environmental conditions for RI event are the same between these two VMX_{start} groups while favorable storm-related conditions for RI event are not. Thus, the comparison on storm-related variables between RI and SI events in the

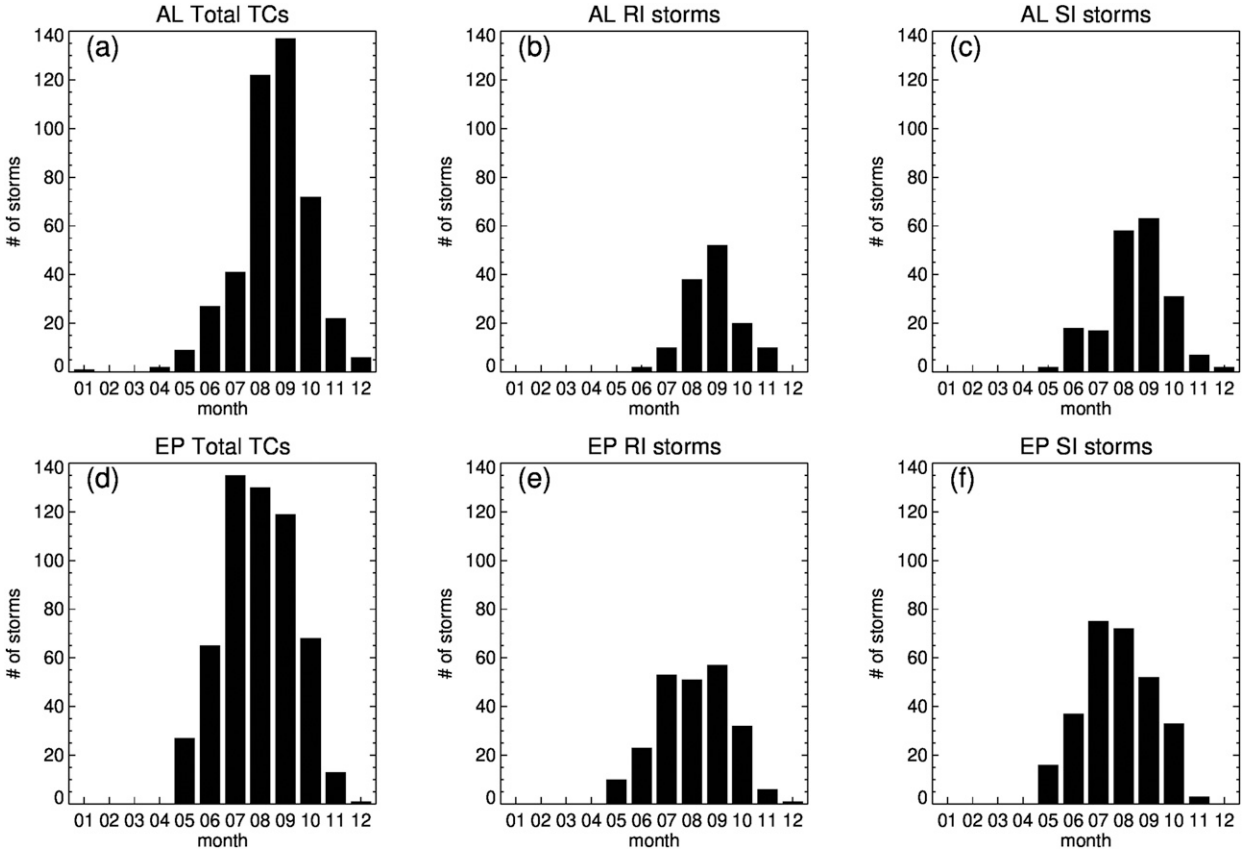

FIG. 4. Monthly distribution of the number of (a) all TCs in AL, (b) RI storms in AL, (c) SI storms in AL, (d) all TCs in EP, (e) RI storms in EP, and (f) SI storms in EP.

three event-relative stages is shown in Table 6 with respect to two VMX_{start} groups, while that of environmental parameters is shown in Table 7 without separating RI/SI events based on VMX_{start}. To first obtain a qualitative picture of how the environmental conditions evolve during RI and SI event, the time evolutions of composite storm-related variables are shown in Fig. 7 for the two VMX_{start} groups. The time evolutions of environmental conditions are shown in Fig. 8 without separating events based on VMX_{start}.

Statistical tests are conducted to better understand differences in the storm-related and environmental conditions for rapidly intensifying events versus those intensifying slowly, based on the composite average values of the parameters listed in Table 5. Statistical testing results are given in Tables 6 and 7. Comparisons are made for before-event, during-event, and event-ending stages of RI events and the corresponding stages of non-RI SI events in order to determine whether or not there exists statistically differences between rapidly intensifying events and slowly intensifying events. A Student's t test was performed for all data in the AL and EP basins, respectively, based on a finding that all the examined parameters are approximately distributed normally. The null hypothesis is that there is no difference in each corresponding stage between RI and SI events (i.e., RI − SI = 0). In this section, a difference is only noted if the confidence level is at or above 95%. Otherwise, similarities will be stated indicating that the null hypothesis was not able to be rejected.

a. Storm-related parameters

Figure 7 presents the comparison of composite evolutions of VMX, LAT, LON, SPD, DVMX, and USTM between RI and SI events for 160 RI and 284 SI events in the AL basin and 268 RI and 386 SI events in the EP basin. Two groups are separated by VMX_{start} as stated above. The numbers of data points in each event-relative stage for each VMX_{start} group and their comparison values and significant test results on the storm-related parameters between RI and SI events are shown in Table 6.

As seen in Table 6 and Fig. 7a, for both VMX_{start} groups, the storm intensity VMX is significantly weaker for RI events than that for SI events in the before-event stage in both AL and EP basins. After events start, the VMX of RI events is significantly stronger than that of SI events in during-event and event-ending stages for both VMX_{start} groups in both basins.

For LAT, during all three event-relative stages in both AL and EP basins, RI events happen significantly farther south than SI events for both VMX_{start} groups (Table 6). Comparing to the AL basin, events in the EP basin are

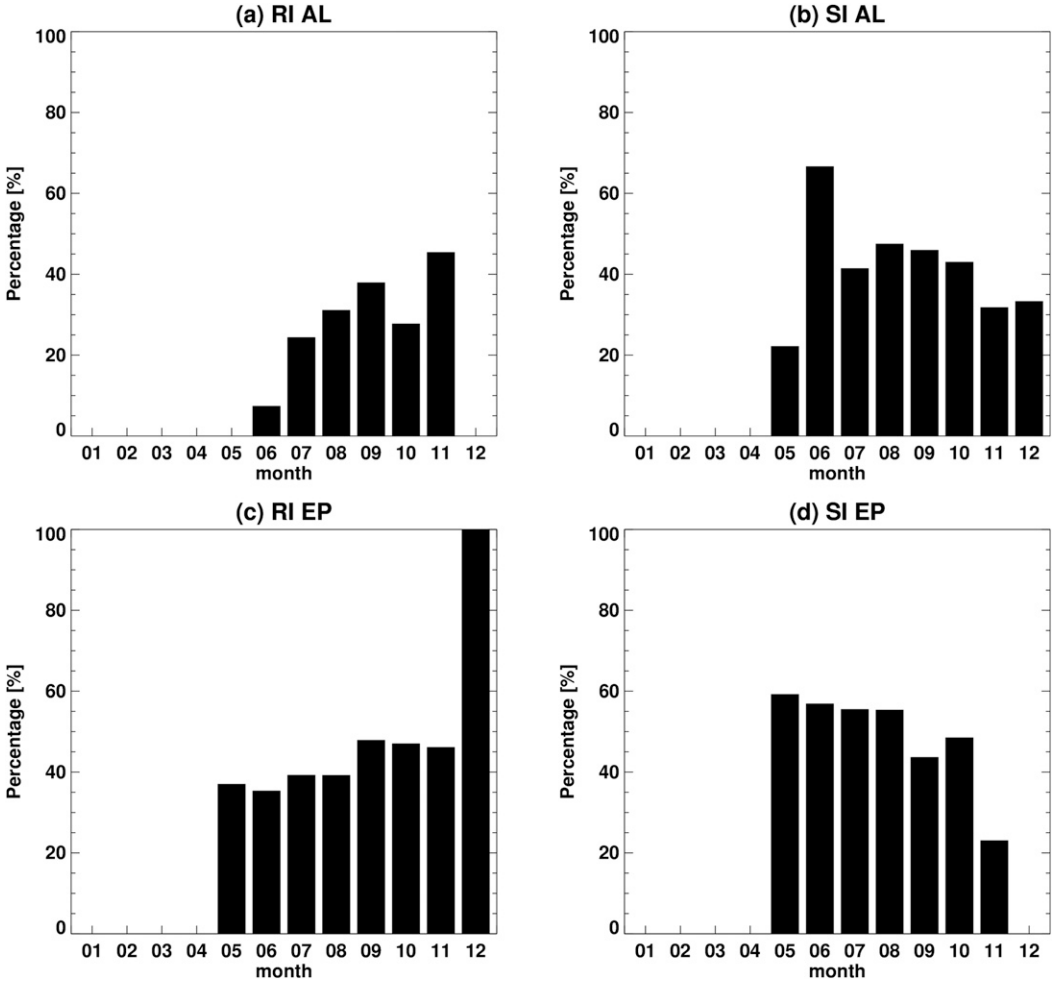

FIG. 5. Monthly distribution of the percentage of TCs that underwent (a) RI in AL, (b) SI in AL, (c) RI in EP, and (d) SI in EP.

located relatively farther south (Fig. 7b). This might be due to the smaller OHC values in EP than AL on average as seen in Table 7 below.

In the AL basin, the differences of LON between RI and SI events are only found to be significant at before-event stage, while no significant differences are found at during-event and event-ending stages. Interestingly, at the before-event stage, RI events of the $VMX_{start} > 40$ kt group are located significantly farther east than SI events of $VMX_{start} > 40$ kt in the AL basin (Fig. 7c). However, at the same stage for the same basin, for the $VMX_{start} \leq 40$ kt group, RI events are located significantly farther west than SI events. In the EP basin, the differences between RI and SI events of $VMX_{start} > 40$ kt at each stage are similar with those in the AL basin, while RI events of $VMX_{start} \leq 40$ kt are located farther east than SI events of the same VMX_{start} group at all three event-relative stages.

For SPD, it is found that for the $VMX_{start} > 40$ kt group, RI storms move significantly faster than SI storms during all three event-relative stages in both basins except for the before-event stage in the EP basin (Table 6, Fig. 7d). However, for the $VMX_{start} \leq 40$ kt group, RI storms move at a similar speed with SI storms at most stages in both basins, except that they move significantly slower than SI storms at the before-event stage in the AL basin ($-0.9\,m\,s^{-1}$) and significantly faster at the during-event stage in the EP basin ($+0.3\,m\,s^{-1}$).

For DVMX, RI events always intensify significantly faster during the previous 12 h than SI events in all the event-relative stages for both VMX_{start} groups and both AL and EP basins. The differences of DVMX between RI and SI events increase from 1–4 kt in the before-event stage to 10–13 kt in the event-ending stage (Table 6, Fig. 7e).

For USTM, for the $VMX_{start} > 40$ kt group, RI events have a significantly stronger westward motion than SI events during all three event-relative stages for both AL and EP basins. In the AL basin, the magnitude of westward storm motion decreases gradually during the event life cycle for both RI and SI events (Fig. 7f). However, for the $VMX_{start} \leq 40$ kt group, RI and SI events have significantly different USTM values only at the before-event stage, during which RI events have a significantly weaker westward motion than SI

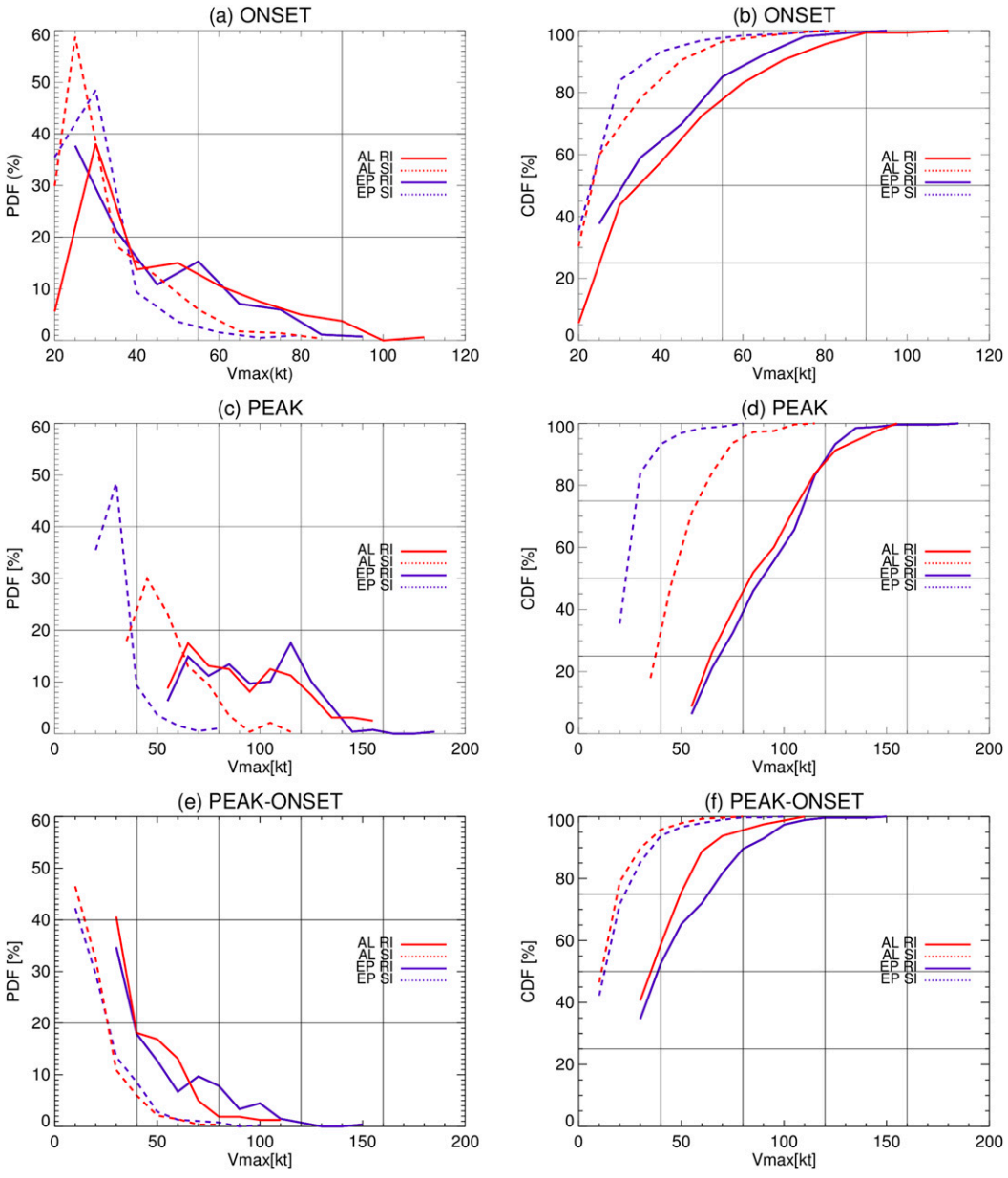

FIG. 6. The probability density function (PDF), and the cumulative density function (CDF) of maximum sustained surface wind (VMX) at (a),(b) RI/SI onset; (c),(d) peak of VMX during RI/SI events; and (e) and (f) difference between VMX at RI/SI onset and the peak VMX value during the RI/SI event for AL and EP RI and SI events.

events in the AL basin but a significantly stronger westward motion in the EP basin.

b. *Environmental parameters*

Figure 8 presents the comparison of composite evolutions of SST, RHLO, RHMD, U200, T200, D200, Z850, EPOS, REFC, SHRD, POT, and OHC between RI and SI events. RI events have significantly warmer SST than SI events for all 3 event-relative stages for both AL and EP basins (Table 7 and Fig. 8a). In the AL, the SSTs for RI events are about 0.4°C warmer for each event-relative stage than those for SI events. In the EP, the SST difference between RI and SI events is 0.52°C in the before-event stage, decreases about 0.1° to 0.4°C in the during-event stage, and increases to 0.61°C in the event-ending stage. The larger variability of SST from the before-event stage to the during-event stage in the EP than the AL basin is consistent with the results by Foltz et al. (2018), which indicated that the SST gradient along TC track in the EP is much larger than that in the AL. This might indicate that the SST plays a more important role in the RI process in the EP

TABLE 6. Mean value of RI events, mean value of SI events, and the mean value differences of the storm-related variables between RI events and SI events for before-event, during-event, and event-ending stages.

			Before-event			During-event			Event-ending		
Category	Event group	Basin	RI	SI	RI − SI	RI	SI	RI − SI	RI	SI	RI − SI
Sample size	$VMX_{start} > 40$ kt	AL	431	191		249	188		239	211	
		EP	649	229		317	168		410	286	
	$VMX_{start} \leq 40$ kt	AL	182	350		199	822		161	409	
		EP	344	495		616	1464		441	889	
VMX	$VMX_{start} > 40$ kt	AL	49.86	56.78	−6.92[c]	68.88	58.70	10.18[c]	95.25	60.88	34.37[c]
		EP	50.68	54.39	−3.71[c]	65.91	55.09	10.82[c]	89.85	59.72	30.13[c]
	$VMX_{start} \leq 40$ kt	AL	30.89	33.70	−2.81[c]	39.65	37.52	2.13[a]	62.08	46.03	16.05[c]
		EP	29.45	31.39	−1.94[c]	47.27	38.42	8.85[c]	80.14	48.86	31.28[c]
LAT	$VMX_{start} > 40$ kt	AL	17.05	21.00	−3.95[c]	18.63	24.18	−5.55[c]	19.27	22.96	−3.69[c]
		EP	13.64	16.20	−2.56[c]	14.33	16.44	−2.11[c]	15.04	16.40	−1.36[c]
	$VMX_{start} \leq 40$ kt	AL	17.68	18.88	−1.20[a]	18.03	20.02	−1.99[c]	19.10	19.34	−0.24[a]
		EP	12.79	14.16	−1.37[c]	13.57	14.55	−0.98[c]	15.15	15.95	−0.80[c]
LON	$VMX_{start} > 40$ kt	AL	−58.46	−63.50	5.04[c]	−65.37	−65.37	0.00	−63.04	−62.44	−0.60
		EP	−111.05	−116.26	5.21[c]	−114.48	−116.58	2.10	−117.22	−115.71	−1.51
	$VMX_{start} \leq 40$ kt	AL	−57.50	−52.44	−5.06[a]	−60.59	−60.89	0.30	−57.36	−54.73	−2.63
		EP	−108.98	−112.37	3.39[c]	−109.53	−111.03	1.50[b]	−110.76	−115.06	4.30[c]
SPD	$VMX_{start} > 40$ kt	AL	5.84	4.78	1.06[c]	5.49	4.75	0.74[b]	5.72	4.85	0.87[c]
		EP	4.36	4.26	0.10	4.94	4.12	0.82[c]	4.83	4.52	0.31[a]
	$VMX_{start} \leq 40$ kt	AL	4.24	5.13	−0.89[c]	4.98	5.01	−0.03	5.52	5.65	−0.13
		EP	3.91	3.77	0.14	4.70	4.40	0.30[b]	4.71	4.64	0.07
DVMX	$VMX_{start} > 40$ kt	AL	6.70	3.18	3.52[c]	9.61	3.10	6.51[c]	19.18	6.88	12.30[c]
		EP	6.61	4.12	2.49[c]	9.81	1.13	8.68[c]	18.33	7.37	10.96[c]
	$VMX_{start} \leq 40$ kt	AL	1.63	0.27	1.36[a]	8.64	5.27	3.37[c]	16.96	6.89	10.07[c]
		EP	2.50	0.88	1.62[c]	12.97	5.87	7.10[c]	20.00	7.58	12.42[c]
USTM	$VMX_{start} > 40$ kt	AL	−4.98	−2.89	−2.09[c]	−4.00	−1.73	−2.27[c]	−3.81	−1.57	−2.24[c]
		EP	−4.10	−3.75	−0.35[a]	−4.52	−3.39	−1.13[c]	−4.21	−3.84	−0.37[a]
	$VMX_{start} \leq 40$ kt	AL	−3.52	−4.29	0.77[a]	−3.71	−3.20	−0.51	−3.20	−3.35	0.15
		EP	−4.06	−3.35	−0.71[c]	−4.08	−4.06	−0.02	−3.75	−3.67	−0.08

[a] Statistical significance of the difference is at the 95% (p value = 0.05) confidence level.
[b] Statistical significance of the difference is at the 99% (p value = 0.01) confidence level.
[c] Statistical significance of the difference is at the 99.9% (p value = 0.001) confidence level.

than in the AL basin. Comparing both basins, not surprisingly, we see that the SSTs in the EP are warmer than SSTs in the AL for RI and SI events, respectively, for the before-event and during-event stages, although this basin-dependent differences are much smaller than the differences between SI and RI events (Table 7).

The relative humidity appears to be important for convective activity, which has been found in a close relationship with rapidly intensifying TCs (TJZ17). In the AL basin, RI events have significantly larger RHLO and RHMD than SI events in all event-relative stages (Table 7). In the EP basin, RI events have similar RHLO and RHMD with SI events for the during-event stage, while RHLO and RHMD of RI events are significantly larger than those of SI events in before-event and event-ending stages (Table 7). Comparing both basins, the EP basin is moister than the AL basin at both low and midlevels for both RI and SI events (Figs. 8b,c).

The U200 represents the zonal flow of environmental wind at 200 hPa (Fig. 8d). Interestingly, on average, SI events in the AL appears to have westerly flow at 200 hPa while RI events in the AL and RI and SI events in the EP have easterly flow. Similarly, previous studies found that the easterly environmental flow at 200 hPa is more likely to appear in RI storms in both the AL basin (KD03) and the northwestern Pacific basin (Shu et al. 2012). In the AL, easterly flow at 200 hPa becomes weaker from before-RI to RI-ending stage while no such trend is found for SI events. The U200 between RI and SI events is significantly different in the AL basin (Table 7). In the EP, SI events have significantly stronger easterly flow than RI events in all event-relative stages (Table 7). In comparing between basins, U200 is stronger for EP events than AL events.

From Fig. 8e, in both basins, there are progressions of warming T200 from the before-event stage to the event-ending stage in both RI and SI events. A warmer T200 might be associated with upper-level high pressure and cause divergence at the upper level. This could lead to surface convergence and further trigger TC intensification. RI events in both basins have significantly warmer T200 than their SI counterparts (Table 7). Comparing both basins, the T200 of RI and SI events in the EP are warmer than those of RI and SI events in the AL, respectively.

RI events appear to have significantly larger D200 than SI events for each event-relative stage for both basins (Table 7). Higher upper-level divergence could lead to larger surface

TABLE 7. Mean value of RI events, mean value of SI events, and the mean value differences of the environmental variables between RI events and SI events for before-event, during-event, and event-ending stages.

		Before-event			During-event			Event-ending		
Category	Basin	RI	SI	RI-SI	RI	SI	RI-SI	RI	SI	RI-SI
SST	AL	28.51	28.08	0.43[c]	28.70	28.31	0.39[c]	28.41	27.97	0.44[c]
	EP	28.75	28.23	0.52[c]	28.84	28.44	0.40[c]	28.42	27.81	0.61[c]
RHLO	AL	73.55	69.04	4.51[c]	72.58	70.25	2.33[c]	71.59	68.63	2.96[c]
	EP	78.32	76.86	1.46[c]	77.82	77.69	0.13	76.38	75.17	1.21[c]
RHMD	AL	62.78	57.17	5.61[c]	61.79	59.41	2.38[c]	59.77	56.82	2.95[c]
	EP	71.30	68.67	2.63[c]	71.01	70.84	0.17	68.43	67.16	1.27[b]
U200	AL	−4.84	3.10	−7.94[c]	−2.55	2.06	−4.61[c]	−0.41	5.67	−6.08[c]
	EP	−9.45	−10.70	1.25[b]	−8.41	−9.36	0.95[c]	−7.21	−8.13	0.92[b]
T200	AL	−53.49	−53.90	0.41[c]	−53.39	−53.77	0.38[c]	−53.32	−53.76	0.44[c]
	EP	−53.24	−53.35	0.11[a]	−53.09	−53.23	0.14[c]	−52.88	−53.08	0.20[c]
D200	AL	4.79	2.85	1.94[c]	4.78	3.81	0.97[c]	5.49	3.73	1.76[c]
	EP	6.80	5.29	1.51[c]	7.07	5.99	1.08[c]	6.24	4.59	1.65[c]
Z850	AL	4.20	2.05	2.15[c]	4.01	2.85	1.16[c]	4.11	2.42	1.69[c]
	EP	2.26	1.90	0.36	2.47	2.51	−0.04	2.93	2.48	0.45[b]
EPOS	AL	9.62	9.50	0.12	9.90	9.36	0.54[c]	9.87	9.23	0.64[c]
	EP	8.11	7.86	0.25[b]	8.14	7.82	0.32[c]	7.76	7.10	0.66[c]
REFC	AL	1.22	1.47	−0.25	1.18	2.27	−1.09[c]	1.51	2.98	−1.47[b]
	EP	−0.74	−0.47	−0.27	−0.82	−0.89	0.07	−0.76	−0.71	−0.05
SHRD	AL	11.91	16.73	−4.82[c]	11.43	14.64	−3.21[c]	13.12	18.14	−5.02[c]
	EP	11.01	13.24	−2.23[c]	9.21	11.56	−2.35[c]	9.61	11.85	−2.24[c]
POT	AL	94.03	91.82	2.21	85.27	95.02	−9.7.5[c]	55.15	79.81	−24.66[c]
	EP	101.06	95.85	5.21[c]	91.94	97.52	−5.58[c]	52.68	72.94	−20.26[c]
OHC	AL	48.77	39.35	9.42[c]	51.02	41.16	9.86[c]	48.56	35.63	12.93[c]
	EP	31.93	26.70	5.23[c]	33.77	27.66	6.11[c]	27.93	20.65	7.28[c]

[a] Statistical significance of the difference is at the 95% (p value = 0.05) confidence level.
[b] Statistical significance of the difference is at the 99% (p value = 0.01) confidence level.
[c] Statistical significance of the difference is at the 99.9% (p value = 0.001) confidence level.

convergence that favors storm intensification. In comparing the two basins, events in the EP have larger magnitudes of upper-level divergence than those in the AL (Fig. 8f).

Higher vorticity at 850 hPa (Z850) represents the intensity of environmental low-level vortex. In the AL, the averaged value of Z850 in RI events is significantly larger than that in SI events for all event-relative stages and it is at least twice as large as that in SI events (Table 7). However, in the EP, no statistically significant differences of Z850 between RI and SI events are found in the before-event and during-event stages while RI events have significantly larger 850-hPa relative vorticity than SI events in the event-ending stage. In comparing the two basins, RI events in the AL have almost twice larger Z580 values than those in the EP (Fig. 8g). This indicates that the environmental vorticity plays a more important role for RI events in AL than EP.

EPOS, the averaged positive difference of the equivalent potential temperatures between a parcel lifted from surface and its environment, averaged between 200 and 800 km from the storm center is shown in Fig. 8h. EPOS measures the convective instability of the TC environment. The storm environment of RI events is significantly more unstable than SI events in during-event and event-ending stages in the AL and in all three event-relative stages in the EP, while no significant difference in the environmental convective instability between RI and SI events is found in the before-event stage in the AL basin. In comparing both basins, the environment of RI and SI events in the AL is more unstable (averaged EPOS value between 9.23° and 9.90°C, Table 7) than that in the EP (averaged EPOS value between 7.10° and 8.14°C).

In the AL, the relative eddy momentum flux convergence (REFC) of RI events is significantly weaker ($-1\,\mathrm{m\,s^{-1}\,day^{-1}}$) than SI events in the during-event stage and the event-ending stage. This agrees with KD03 who showed that most of RI cases in the AL were associated with weak REFC. However, the REFC of RI events is similar with that of SI events in the before-event stage in the AL and in all three event-relative stages in the EP (Table 7). In the AL, both RI and SI events have positive values of REFC. But in the EP, the REFC values are generally negative for both RI and SI events (Fig. 8i). Previous studies indicated that positive value of REFC may trigger an inward-propagating maximum TC radial wind, which may cause a secondary eyewall formation and make TC temporarily weakening (Molinari and Vollaro 1989, 1990). This indicate that the EP environment might not be favorable for the eyewall replacement.

The environmental vertical wind shear (SHRD) is deemed as one of the most important predictors in RI forecasting (DeMaria and Kaplan 1999; KD03; Kaplan et al. 2010; Shu et al. 2012). Low to medium shear values are very important for RI. SHRD is significantly weaker for RI events than that for SI events in both basins (Table 7). Additionally, the difference

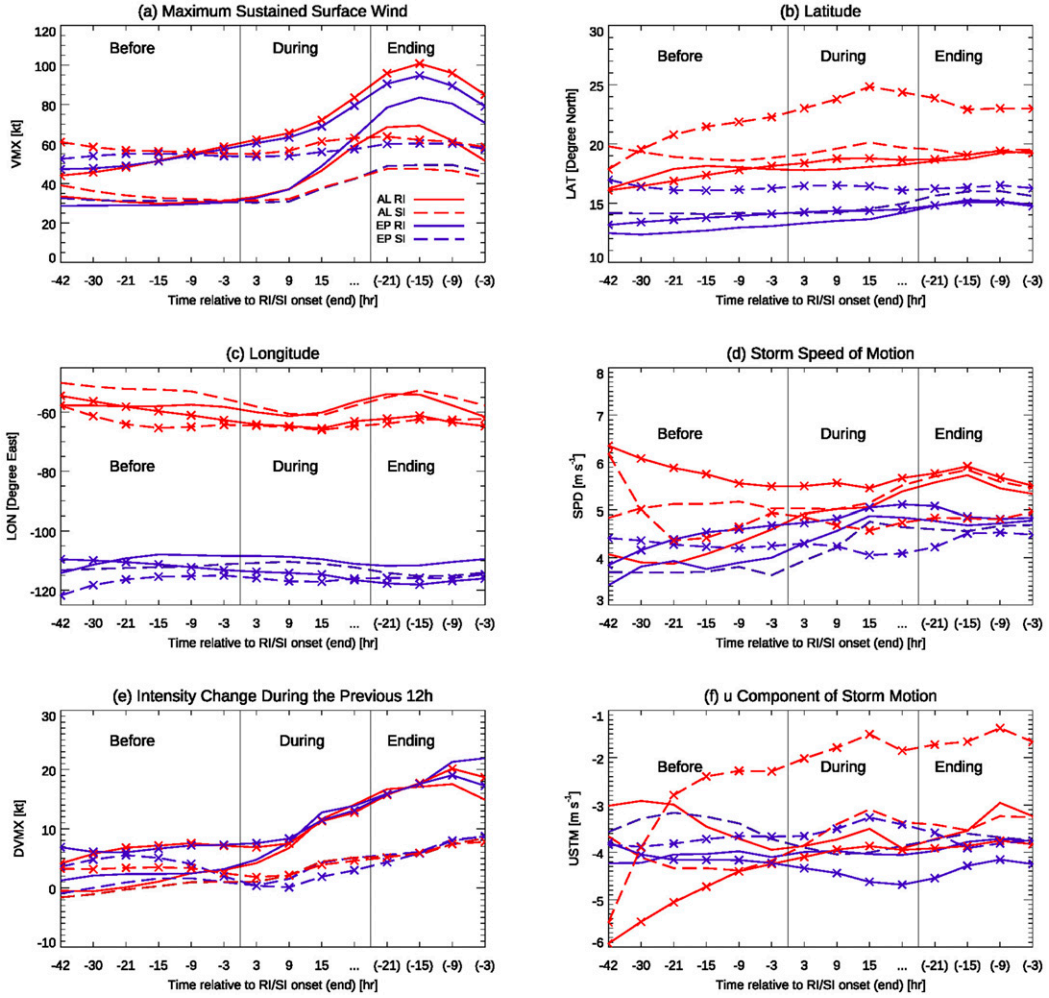

FIG. 7. Time evolution of composite (a) VMX (kt), (b) LAT (°N), (c) LON (°E), (d) SPD ($m\,s^{-1}$), (e) DVMX (kt), and (f) USTM ($m\,s^{-1}$) during RI and SI events in AL and EP basins during 1982–2016. Lines without "×" represent events of $VMX_{start} \leq 40$ kt. Lines with "×" represent events of $VMX_{start} > 40$ kt.

between RI events and SI events is less in the EP than in the AL. In the AL, the shear decreases to its lowest level in the during-event stage, and then increases in the event-ending stage to a relatively high level again. Comparing both basins, during the whole event life cycle, the SHRD in the AL is typically stronger than that in the EP basin.

Figure 8k shows the evolution of POT, which measures how far the storm maximum potential intensity is beyond than its current intensity. At the before-event stage, no significantly difference of POT between RI and SI events is found in the AL basin, while RI events in the EP has significantly larger value of POT than SI events (Table 7). As the storm intensity increases rapidly, significantly smaller POT value for RI event is found than that for SI events in the during-event and event-ending stages (Table 7). Comparing both basins, the POT values are generally larger for both RI and SI events in the EP than those in the AL, indicating that EP storms have higher potential to intensify rapidly.

Figure 8l shows the evolution of OHC, which combines the upper-ocean and SST information into a single parameter (Mainelli et al. 2008). The maximum OHC appears in the during-event stage for both RI and SI events. In both basins, RI events are associated with a significantly larger OHC than SI events in all three event-relative stages (Table 7). Comparing the two basins, averaged OHC values of RI and SI events in the AL are much larger than those in the EP for all three event-relative stages. This is consistent with previous studies suggesting that the gradient of OHC along TC track in the AL is larger than in the Pacific (Foltz et al. 2018). Larger OHC gradient can directly cause air-sea interaction, which lead TCs to undergoing RI events. Combined with the finding of drier low- to midlevel relative humidity in the AL than that in the EP, this seems suggest that RI in the EP more likely happens by using water vapor contained in the atmosphere, while the air in the AL has less vapor and RI in the AL relies more on energies from the ocean.

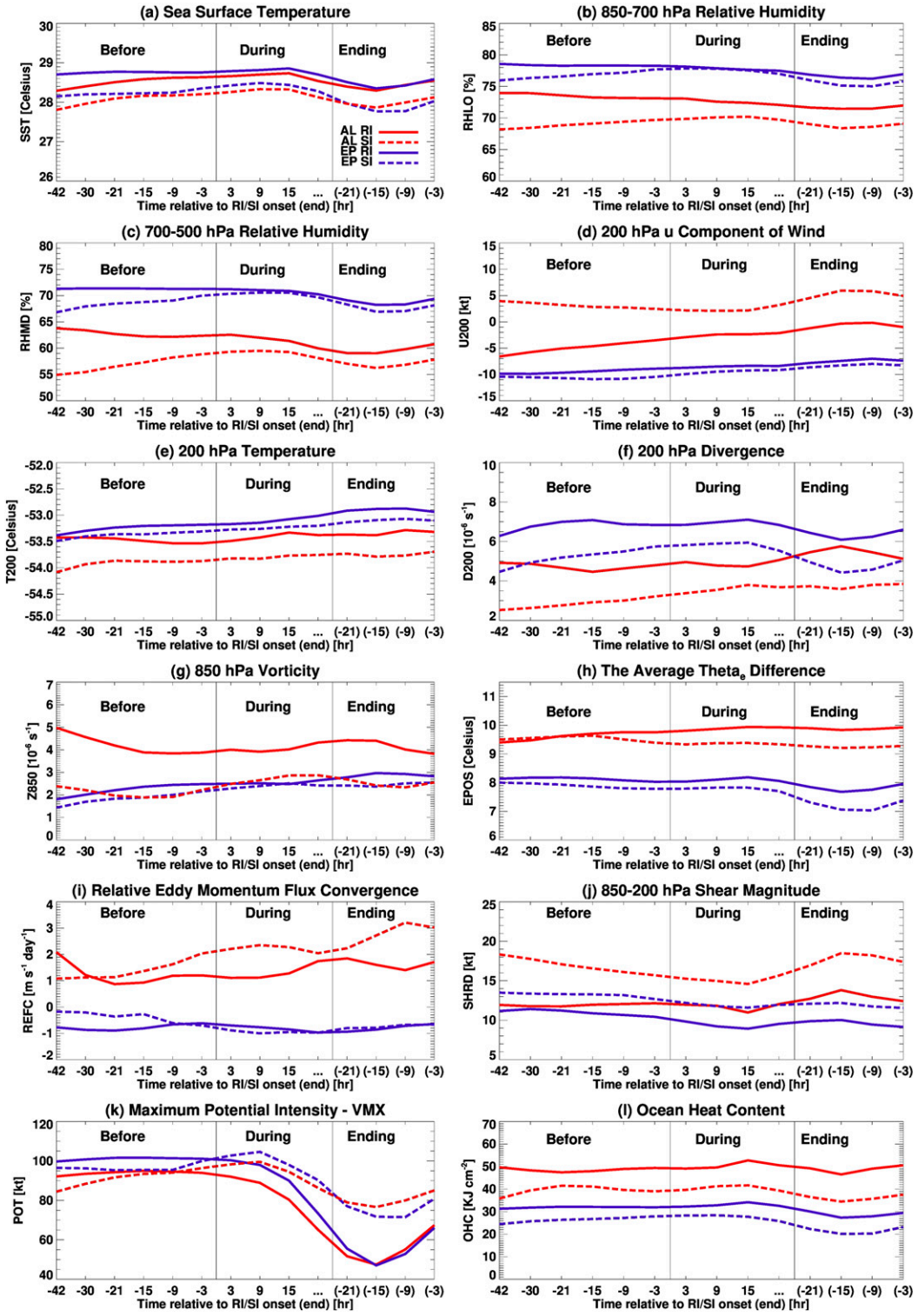

FIG. 8. Time evolution of composite (a) SST (°C), (b) RHLO (%), (c) RHMD (%), (d) U200 (kt), (e) T200 (°C), (f) D200 (10^{-6} s^{-1}), (g) Z850 (10^{-6} s^{-1}), (h) EPOS (°C), (i) REFC (m s^{-1} day^{-1}), (j) SHRD (kt), (k) POT (kt), and (l) OHC (KJ cm^{-2}) during RI and SI events in AL and EP basins during 1982–2016.

To sum up, statistically significant differences are found for most of large-scale environmental parameters examined in this study between some or all 3 corresponding stages of RI events and SI events in the AL and EP basins. These parameters included SST, RHLO, RHMD, U200, T200, D200, Z850, EPOS, SHRD, POT, and OHC. The result is quite different when comparing with previous related studies such as HPFL10. HPFL10 studied environmental and storm-related characteristics of RI and SI cases in the AL and WP basins from 2003 to 2008 (6 years). They only found that RI cases occurred in environments with significantly larger conditional instability than SI cases in the WP, and with weaker deep-layer shear than SI cases in the AL. All other environmental parameters examined in HPFL10 were found to be similar between RI and SI cases in the AL and WP. However, this study found more significantly differences between RI and SI events when comparing their corresponding stages. The reason is threefold: 1) the small sample size that HPFL10 used is small. In their study, there are only 181 cases and 36 RI cases in the AL and 436 SI cases and 81 RI cases in the WP during the 6-yr (2003–08) study period. 2) HPFL10 (as well as KD03; Shu et al. 2012) defined RI and SI using a case-based definition, while this study uses a more realistic event-based definition for RI and SI as mentioned in the introduction. 3) Another potential reason might be that HPFL10 used a different analysis Navy Operational Global Atmospheric Prediction System to create the composite of environment of TCs, which is different with SHIPS database in this study.

5. Conclusions

Based on the 35-yr (1982–2016) HURDAT2 data and SHIPS developmental database, this study examined the climatology of RI and SI storms and events as well as the time evolutions of storm-related, and environmental parameters for RI and SI events in both AL and EP basins. By following TJZ17, each RI event is defined as multiple, continuous and overlapping 24-h RI cases. Each RI case is a 24-h period during which $\Delta V_{\max 24} \geq 30$ kt as in KD03. Similarly, we define each SI event as multiple, continuous and overlapping 24-h SI cases, which are 24-h periods with $10 \leq \Delta V_{\max 24} \leq 30$ kt. Totally, 997 TCs including 439 in the AL and 558 in the EP are examined in this study, from which 160 RI and 284 SI events in the AL basin and 268 RI and 386 SI events in the EP basin are identified.

Concerning the climatology of RI and SI storms, it is found that 90% of all major hurricanes, 44% of all CAT12 hurricanes, and 2% of all TD/TS systems underwent RI, while 10% of all major hurricanes, 48% of all CAT12 hurricanes, and 72% of all TD/TS systems underwent SI. Major hurricanes were intensified mainly through undergoing RI while TD/TS systems were intensified mainly through SI. About a half of CAT12 hurricanes intensified through RI and another half through SI. The majority of RI/SI events last more than 24 h. The maximum length of an RI event is 78 h, while the maximum length of an SI event is 144 h. This strongly suggests the necessity of treating RI and SI as events when examining the evolution of RI/SI.

Seasonally, in the AL basin, the total number of TCs peaks in September, followed by August and October. So does the number of RI storms and that of SI storms. In the EP basin, both of numbers of all TCs and SI storms peak in July, followed by August and September. But the number of RI storms peaks in September instead, followed by July and August. Interestingly, the percentage of TCs that underwent RI peaks late in the hurricane season, November in AL and December in EP (Figs. 5a,c), while the percentage of SI storms peaks early in the season, June in AL and May in EP (Figs. 5b,d).

For the first time in the literature, we found that RI events have significantly different storm-related and environmental characteristics than SI events for in both AL and EP basins. These differences appear in all 6 storm-related (VMX, LAT, LON, SPD, DVMX, and USTM) and 12 environmental parameters (SST, RHLO, RHMD, U200, T200, D200, Z850, EPOS, REFC, SHRD, POT, and OHC) examined in this study for either some or all three event-relative stages between RI and SI.

When comparing the evolution of storm-related parameters between different stages of RI and SI events, we found that the TC intensity of an RI event is significantly weaker in the before-event stage and stronger in during-event and event-ending stages than that of a SI event in both AL and EP basins. RI events are located farther south and always intensify faster during the previous 12 h than SI events during all three event-relative stages in both basins. A few favorable storm-related parameters, including LON, SPD, and USTM, for RI events compared to SI events are found to be different between events with a weak onset intensity ($\mathrm{VMX_{start}} \leq 40$ kt) and those with a strong onset intensity ($\mathrm{VMX_{start}} > 40$ kt). For the $\mathrm{VMX_{start}} > 40$ kt event group in both AL and EP basins, RI events appear to be farther east than SI events in the before-event stage, move significantly faster than SI events during all three event-relative stages except for the before-event stage in the EP basin, and have a significantly stronger westward motion than SI events during all three event-relative stages. But for the $\mathrm{VMX_{start}} \leq 40$ kt group, the following is true: 1) in the AL, RI events appear to be farther west in the before-event stage than SI events, while in the EP, RI events appear to be farther east than SI events in all three event-relative stages. 2) RI storms move significantly slower than SI storms at the before-event stage in the AL basin and significantly faster at the during-event stage in the EP basin. 3) RI and SI events have significantly different USTM values only at the before-event stage, during which RI events have a significantly weaker westward motion than SI events in the AL basin but a significantly stronger westward motion in the EP basin.

When comparing the evolution of environmental parameters between different stages of RI and SI events, we found that the RI events have significantly warmer SST than SI events for all 3 event-relative stages. In the AL, RI events have significantly larger low-level and midlevel relative humidity than SI events in all event-relative stages. In the EP, RI events have similar low-level and midlevel relative humidity with SI events for the during-event stage, while RHLO and RHMD of RI events are significantly larger than those of SI events in before-event and event-ending stages. In the AL, the environmental flow at 200 hPa for RI events is easterly while that of SI events is westerly for all three event-relative stages. In the EP, both RI

and SI events have easterly flow at 200 hPa on average and this easterly flow is significantly weaker for in RI events than in SI events. RI events have significantly warmer 200-hPa temperatures and significantly larger 200-hPa divergence than SI events in all event-relative stages in both AL and EP basins. In the AL, RI events have significantly larger 850-hPa relative vorticity than SI events for all event-relative stages. However, in the EP, there are no statistically significant differences of 850-hPa relative vorticity between RI and SI events in before-event and during-event stages. RI events in the EP have significantly larger 850-hPa relative vorticity than SI events in the event-ending stage. RI events is more unstable than SI events in during-event and event-ending stages in the AL and in all three event-relative stages in the EP. In the AL, the relative eddy momentum flux convergence of RI events is significantly weaker than SI events in the during-event stage and the event-ending stage. However, the REFC of RI events is similar with that of SI events in the before-event stage in the AL and in all three event-relative stages in the EP. In both basins, the environmental vertical wind shear of RI events is significantly weaker than SI events for each event-relative stage. In the AL, there is no significant difference of POT between RI and SI events in the before-event stage. However, in the same stage, RI events in the EP has significantly larger value of POT than SI events. On the other hand, RI events have significantly smaller POT values than SI events in during-event and event-ending stages in both basins. In both basins, the ocean heat content of RI events is significantly greater than that of SI events for all three event-relative stages.

In summary, for all environmental characteristics examined in this study, RI events are found to have a more favorable environmental condition for TC intensification than SI events. An environment with significantly warmer SST, lower environmental vertical wind shear, higher relative humidity in low to midlevels, warmer 200-hPa temperature, larger 200-hPa divergence, or greater ocean heat content seems favorable for RI events in both AL and EP basins. However, there are some basin-dependent differences. In the EP, a set of favorable atmosphere conditions including weak shear, strong D200, low REFC, high SST, moist air at low to middle atmosphere, and a high POT value is more readily available for RI than the AL basin. In the AL, the contribution of SST is found to be relatively weaker (Foltz et al. 2018) and RHLO and RHMD is found to be drier than in the EP basin. The AL basin has larger ocean heat content, higher EPOS, and stronger Z850, which are more important for RI events in this basin.

HPFL10 found that the environmental variables between RI and SI cases in the WP and AL basins for a 6-yr period (2003–08) are quite similar except that RI cases occurred in environments with significantly larger conditional instability than SI cases in the WP basin and weaker deep-layer shear than in the AL basin. However, this study, using a much longer period of data (35 years, 1982–2016) and a new event-based RI/SI definition, found for the first time that most of the environmental and storm-related characteristics are significantly different between RI and SI events in the AL and EP basins. This finding could be applied to future RI forecasting schemes, especially for differentiating RI and SI based on environmental conditions.

Acknowledgments. The authors thank Dr. Mark DeMaria for helpful discussions about SHIPS parameters. We also thank three anonymous reviewers for their helpful comments, which lead to substantial improvement of the manuscript. This research was supported by NASA Weather And Atmospheric Dynamics (WAAD) Grant NNX17AH72G under the direction of Drs. Ramesh Kakar and Gail Jackson and NOAA Joint Hurricane Testbed (JHT) Grants NA15OAR4590199 and NA17OAR4590142 under the direction of Mr. Richard Fulton and Dr. Chris Landsea. The data used in this study are listed in the references, tables, and figures.

REFERENCES

Alvey, G., III, J. Zawislak, and E. J. Zipser, 2015: Precipitation properties observed during tropical cyclone intensity change. *Mon. Wea. Rev.*, **143**, 4476–4492, https://doi.org/10.1175/MWR-D-15-0065.1.

Bukunt, B. P., and G. M. Barnes, 2015: The subtropical jet stream delivers the coup de grâce to Hurricane Felicia (2009). *Wea. Forecasting*, **30**, 1039–1049, https://doi.org/10.1175/WAF-D-15-0004.1.

Chan, J. C.-L., and R. T. Williams, 1987: Analytical and numerical studies of the beta-effect in tropical cyclone motion. Part I: Zero mean flow. *J. Atmos. Sci.*, **44**, 1257–1265, https://doi.org/10.1175/1520-0469(1987)044<1257:AANSOT>2.0.CO;2.

DeMaria, M., 2010: Tropical cyclone intensity change predictability estimates using a statistical-dynamical model. *29th Conf. on Hurricanes and Tropical Meteorology,* Tucson, AZ, Amer. Meteor. Soc., 9C.5, https://ams.confex.com/ams/29Hurricanes/techprogram/paper_167916.htm.

——, and J. Kaplan, 1994: A Statistical Hurricane Intensity Prediction Scheme (SHIPS) for the Atlantic basin. *Wea. Forecasting*, **9**, 209–220, https://doi.org/10.1175/1520-0434(1994)009<0209:ASHIPS>2.0.CO;2.

——, and ——, 1999: An updated Statistical Hurricane Intensity Prediction Scheme for the Atlantic and eastern North Pacific basins. *Wea. Forecasting*, **14**, 326–337, https://doi.org/10.1175/1520-0434(1999)014<0326:AUSHIP>2.0.CO;2.

——, J.-J. Baik, and J. Kaplan, 1993: Upper-level eddy angular momentum fluxes and tropical cyclone intensity change. *J. Atmos. Sci.*, **50**, 1133–1147, https://doi.org/10.1175/1520-0469(1993)050<1133:ULEAMF>2.0.CO;2.

——, M. Mainelli, L. K. Shay, J. A. Knaff, and J. Kaplan, 2005: Further improvements to the Statistical Hurricane Intensity Prediction Scheme (SHIPS). *Wea. Forecasting*, **20**, 531–543, https://doi.org/10.1175/WAF862.1.

——, R. DeMaria, J. Knaff, and D. Molenar, 2012: Tropical cyclone lightning and rapid intensity change. *Mon. Wea. Rev.*, **140**, 1828–1842, https://doi.org/10.1175/MWR-D-11-00236.1.

——, C. R. Sampson, J. A. Knaff, and K. D. Musgrave, 2014: Is tropical cyclone intensity guidance improving? *Bull. Amer. Meteor. Soc.*, **95**, 387–398, https://doi.org/10.1175/BAMS-D-12-00240.1.

Ditchek, S. D., T. C. Nelson, M. Rosenmayer, and K. L. Corbosiero, 2017: The relationship between tropical cyclones at genesis and their maximum attained intensity. *J. Climate*, **30**, 4897–4913, https://doi.org/10.1175/JCLI-D-16-0554.1.

Foltz, G. R., K. Balaguru, and S. Hagos, 2018: Interbasin differences in the relationship between SST and tropical cyclone intensification. *Mon. Wea. Rev.*, **146**, 853–870, https://doi.org/10.1175/MWR-D-17-0155.1.

Fudeyasu, H., K. Ito, and Y. Miyamoto, 2018: Characteristics of tropical cyclone rapid intensification over the western North

Pacific. *J. Climate*, **31**, 8917–8930, https://doi.org/10.1175/JCLI-D-17-0653.1.

Gu, J., Z. Tan, and X. Qiu, 2016: Quadrant-dependent evolution of low-level tangential wind of a tropical cyclone in the shear flow. *J. Atmos. Sci.*, **73**, 1159–1177, https://doi.org/10.1175/JAS-D-15-0165.1.

Hanley, D., J. Molinari, and D. Keyser, 2001: A composite study of the interactions between tropical cyclones and upper-tropospheric troughs. *Mon. Wea. Rev.*, **129**, 2570–2584, https://doi.org/10.1175/1520-0493(2001)129<2570:ACSOTI>2.0.CO;2.

Hendricks, E. A., M. S. Peng, B. Fu, and T. Li, 2010: Quantifying environmental control on tropical cyclone intensity change. *Mon. Wea. Rev.*, **138**, 3243–3271, https://doi.org/10.1175/2010MWR3185.1.

Holland, G. J., 1983: Tropical cyclone motion: Environmental interaction plus a beta effect. *J. Atmos. Sci.*, **40**, 328–342, https://doi.org/10.1175/1520-0469(1983)040<0328:TCMEIP>2.0.CO;2.

Jiang, H., 2012: The relationship between tropical cyclone intensity change and the strength of inner-core convection. *Mon. Wea. Rev.*, **140**, 1164–1176, https://doi.org/10.1175/MWR-D-11-00134.1.

——, and E. M. Ramirez, 2013: Necessary conditions for tropical cyclone rapid intensification as derived from 11 years of TRMM data. *J. Climate*, **26**, 6459–6470, https://doi.org/10.1175/JCLI-D-12-00432.1.

——, C. Liu, and E. J. Zipser, 2011: A TRMM-based tropical cyclone cloud and precipitation feature database. *J. Appl. Meteor. Climatol.*, **50**, 1255–1274, https://doi.org/10.1175/2011JAMC2662.1.

Judt, F., and S. Chen, 2016: Predictability and dynamics of tropical cyclone rapid intensification deduced from high-resolution stochastic ensembles. *Mon. Wea. Rev.*, **144**, 4395–4420, https://doi.org/10.1175/MWR-D-15-0413.1.

Kaplan, J., and M. DeMaria, 2003: Large-scale characteristics of rapidly intensifying tropical cyclones in the North Atlantic basin. *Wea. Forecasting*, **18**, 1093–1108, https://doi.org10.1175/1520-0434(2003) 018<1093:LCORIT>2.0.CO; 2.

——, ——, and J. Knaff, 2010: A revised tropical cyclone rapid intensification index for the Atlantic and eastern North Pacific basins. *Wea. Forecasting*, **25**, 220–241, https://doi.org/10.1175/2009WAF2222280.1.

——, and Coauthors, 2015: Evaluating environmental impacts on tropical cyclone rapid intensification predictability utilizing statistical models. *Wea. Forecasting*, **30**, 1374–1396, https://doi.org/10.1175/WAF-D-15-0032.1.

Kieper, M. E., and H. Jiang, 2012: Predicting tropical cyclone rapid intensification using the 37 GHz ring pattern identified from passive microwave measurements. *Geophys. Res. Lett.*, **39**, L13804, https://doi.org/10.1029/2012GL052115.

Kowch, R., and K. Emanuel, 2015: Are special processes at work in the rapid intensification of tropical cyclones? *Mon. Wea. Rev.*, **143**, 878–882, https://doi.org/10.1175/MWR-D-14-00360.1.

Landsea, C. W., and J. L. Franklin, 2013: Atlantic hurricane database uncertainty and presentation of a new database format. *Mon. Wea. Rev.*, **141**, 3576–3592, https://doi.org/10.1175/MWR-D-12-00254.1.

Leroux, M.-D., J. Meister, D. Mekies, and P. Caroff, 2018: A climatology of southwest Indian Ocean tropical systems: Their number, tracks, impacts, sizes, empirical maximum potential intensity, and intensity changes. *J. Appl. Meteor. Climatol.*, **57**, 1021–1041, https://doi.org/10.1175/JAMC-D-17-0094.1.

Mainelli, M., M. DeMaria, L. K. Shay, and G. Goni, 2008: Application of oceanic heat content estimation to operational forecasting of recent Atlantic category 5 hurricanes. *Wea. Forecasting*, **23**, 3–16, https://doi.org/10.1175/2007WAF2006111.1.

Merrill, R., 1988: Applied mathematics for earth scientists. *Eos, Trans. Amer. Geophys. Union*, **69**, 637, https://doi.org/10.1029/88EO00205.

Molinari, J., and D. Vollaro, 1989: External influences on hurricane intensity. Part I: Outflow layer eddy angular momentum fluxes. *J. Atmos. Sci.*, **46**, 1093–1105, https://doi.org/10.1175/1520-0469(1989)046<1093:EIOHIP>2.0.CO;2.

——, and ——, 1990: External influences on hurricane intensity. Part II: Vertical structure and response of the hurricane vortex. *J. Atmos. Sci.*, **47**, 1902–1918, https://doi.org/10.1175/1520-0469(1990)047<1902:EIOHIP>2.0.CO;2.

Nguyen, L., and J. Molinari, 2015: Simulation of the downshear reformation of a tropical cyclone. *J. Atmos. Sci.*, **72**, 4529–4551, https://doi.org/10.1175/JAS-D-15-0036.1.

Peirano, C. M., K. L. Corbosiero, and B. H. Tang, 2016: Revisiting trough interactions and tropical cyclone intensity change. *Geophys. Res. Lett.*, **43**, 5509–5515, https://doi.org/10.1002/2016GL069040.

Reynolds, R. W., and T. M. Smith, 1993: An improved real-time global sea surface temperature analysis. *J. Climate*, **6**, 114–119, https://doi.org/10.1175/1520-0442(1993)006<0114:AIRTGS>2.0.CO;2.

Schumacher, A., M. DeMaria, and J. Knaff, 2013: Summary of the new statistical-dynamical intensity forecast models for the Indian Ocean and Southern Hemisphere and resulting performance. JTWC Project Final Rep., 11 pp., https://rammb.cira.colostate.edu/research/tropical_cyclones/ships/docs/JTWC_project_final_report_oct_2013.docx.

Shu, S., J. Ming, and P. Chi, 2012: Large-scale characteristics and probability of rapidly intensifying tropical cyclones in the Western North Pacific basin. *Mon. Wea. Rev.*, **27**, 411–423, https://doi.org/10.1175/WAF-D-11-00042.1.

Simpson, R. H., 1974: The hurricane disaster potential scale. *Weatherwise*, **27**, 169–186, https://doi.org/10.1080/00431672.1974.9931702.

Tao, C., and H. Jiang, 2015: Distributions of shallow to very deep precipitation—Convection in rapidly intensifying tropical cyclones. *J. Climate*, **28**, 8791–8824, https://doi.org/10.1175/JCLI-D-14-00448.1.

——, ——, and J. Zawislak, 2017: The relative importance of stratiform and convective rainfall in rapidly intensifying tropical cyclones. *Mon. Wea. Rev.*, **145**, 795–809, https://doi.org/10.1175/MWR-D-16-0316.1.

Wang, C., X. D. Wang, R. H. Weisberg, and M. Black, 2017: Variability of tropical cyclone rapid intensification in the North Atlantic and its relationship with climate variations. *Climate Dyn.*, **49**, 3627–3645, https://doi.org/10.1007/s00382-017-3537-9.

Wang, X. D., C. Wang, L. Zhang, and X. Wang, 2015: Multidecadal variability of tropical cyclone rapid intensification in the western North Pacific. *J. Climate*, **28**, 3806–3820, https://doi.org/10.1175/JCLI-D-14-00400.1.

Wu, L., H. Su, R. G. Fovell, T. J. Dunkerton, Z. Wang, and B. H. Kahn, 2015: Impact of environmental moisture on tropical cyclone intensification. *Atmos. Chem. Phys.*, **15**, 14 041–14 053, https://doi.org/10.5194/acp-15-14041-2015.

Zagrodnik, J. P., and H. Jiang, 2014: Rainfall, convection, and latent heating distributions in rapidly intensifying tropical cyclones. *J. Atmos. Sci.*, **71**, 2789–2809, https://doi.org/10.1175/JAS-D-13-0314.1.

Zhang, D., L. Zhu, X. Zhang, and V. Tallapragada, 2015: Sensitivity of idealized hurricane intensity and structures under varying background flows and initial vortex intensities to different vertical resolutions in HWRF. *Mon. Wea. Rev.*, **143**, 914–932, https://doi.org/10.1175/MWR-D-14-00102.1.

Zhao, H., X. Duan, G. B. Raga, and P. J. Klotzbach, 2018: Changes in characteristics of rapidly intensifying western North Pacific tropical cyclones related to climate regime shifts. *J. Climate*, **31**, 8163–8179, https://doi.org/10.1175/JCLI-D-18-0029.1.